Structural Engineering and Mechanics, Vol. 21, No. 2 (2005) 151-168

DOI: http://dx.doi.org/10.12989/sem.2005.21.2.151

The buckling of rectangular plates with opening using a polynomial method

T. Muhammad† and A. V. Singh‡

Department of Mechanical and Materials Engineering, The University of Western Ontario, London, Ontario, N6A 5B9, Canada

(Received February 5, 2004, Accepted July 5, 2005)

Abstract. In this paper an energy method is presented for the linear buckling analysis of first order shear deformable plates. The displacement fields are defined in terms of the shape functions, which correspond to a set of predefined points and are composed of significantly high order polynomials. The locations of these points are found by mapping the geometry using the naturalized coordinates and bilinear shape functions. In order to evaluate the method, fully clamped and simply supported rectangular plates subjected to uniform uniaxial compressive loading on two opposite edges of the plate are investigated thoroughly and the results are compared with the exact solution given in the monograph of Timoshenko and Gere (1961). The method is extended to the analysis of perforated plates, wherein the negative stiffness computed over the opening area from in-plane and out-of-plane deformation modes is superimposed to the stiffness of the full plate. Numerical results are then favorably compared with those obtained by finite element methods. Other cases such as; rectangular plates with eccentrically located openings of different shapes are studied and reported in this paper with regards to the effect of aspect ratio, hole size, and hole position on the buckling. For a square plate with a large circular opening at the center, diameter being 80 percent of the length, the present method yields buckling coefficient 12.5 percent higher than the one from the FEM.

Key words: meshless method; perforated plate; *p*-type formulation; buckling; negative stiffness.

1. Introduction

Thin plates are very commonly used in offshore, aerospace, and construction industries. Common examples are bottom and deck of ship structures, platforms of offshore structures, and plate and box girders of bridges. Plates in such structures are often subjected to axial compressive loadings, which can produce the instability. In many cases these plates contain holes for maintenance, inspection, and service operations. Since these holes increase the possibility of instability, many researchers have worked on the buckling of perforated plates over the past few decades. Yettram and Brown (1985, 1986) published two papers on the buckling of square perforated plates using conjugate load/displacement method. Finite element method based on strain fields, was used by Sabir and Chow (1983, 1986) to examine the elastic buckling of plates with eccentrically located circular holes. The conjugate load/displacement method was used again by Shakerley and Brown (1996) for the

† Research Associate
‡ Associate Professor, Corresponding author, E-mail: avsingh@eng.uwo.ca

buckling of plates with eccentrically positioned rectangular openings. A parametric study was presented by El-Sawy and Nazmy (2001) using the finite element computer code ANSYS. They examined the effect of aspect ratio on the elastic buckling of plates with eccentric holes. Differential quadrature method has recently been developed for the vibration analysis of cylindrical shells by Bert and Malik (1996) and been further extended to the buckling of cylindrical shell panels by Redekop and Makhoul (2001).

Finite element method became the widely accepted solution method for engineering problems and is being improved for a variety of new applications together with improved accuracy. In the recent years, meshless solution method has received a lot of attention of many researchers. A series of papers has been published by Belytschko and co workers (1994, 1996) on element free Galerkin method. El. Ouatouati and Johnson (1999) presented a method using a meshless spatial approximation based only on nodes to derive the stiffness and mass matrices for a three dimensional simply connected elastic body. An element free method using Lagrange polynomial without employing the moving least square (MLS) was used by Suetake (2002) and the paper discussed the solutions of elastic beam and plate problems. Mohr (2000) used a least square approach for the approximate polynomial solutions for simply supported equilateral and square plates. An element free Galerkin method was proposed by Chen *et al.* (2003) for the free vibration analysis of laminated composite plates. They considered square, elliptical and perforated plates as numerical examples. Muhammad and Singh (2003) used a meshless method based on the Work-Energy principle for the bending of plates and studied doubly connected rectangular, circular, and elliptical plates as numerical examples.

In the present work buckling of a plate with or without opening is examined by a single-domain-method which is a modified version of the Ritz method and based on the Work-Energy principle. The geometry of the plate is defined by four straight edges wherein the coordinates of the four corner points are prescribed. Then the shape functions in terms of the natural coordinates are used to generate a set of equally spaced nodal points which are used as displacement nodes. The displacement fields in the Cartesian coordinates are then derived in polynomials and their order depends on the number of displacement nodes just mentioned above. First the stiffness matrix including both in-plane and out-of-plane deflection modes is obtained for the full plate. Next the stiffness matrix of the opening part of the plate is obtained using the same displacement fields and set of degrees of freedom as the ones used for the full plate and is subtracted from the first part to obtain the stiffness matrix for the perforated plate. Integration for this is carried out by Gauss-method for which the number of integration points and corresponding weights are selected according to the order of the displacement shape functions. Rectangular plates with both simply supported and clamped edge boundary conditions have been solved by the present method with various types of openings. Results from the present method are compared favorably with the exact solution (Tikmoshenko and Gere 1961), results in the literature (El-Sawy and Nazmy 2001), and the finite element solution (I-DEAS). A parametric study is also presented to investigate the effects of the aspect ratio, hole-size, and hole-location along the diagonal of the plate, on the stability of the rectangular plates.

2. Plate equations

The equations in this section are based on the Reissner-Mindlin theory of plates that is also known as the first order shear deformation theory. The displacement components along the Cartesian axes at an arbitrary point in the plate are denoted by u', v', and w' respectively and are expressed as:

$$u' = u + z\beta_1, \quad v' = v + z\beta_2, \quad w' = w \tag{1}$$

In the above, symbols u, v, and w denote the displacement components at the middle plane of the plate in x, y, and z directions respectively; β_1 and β_2 are the components of rotation of the normal to the middle plane; and z is the distance measured along the normal from the middle plane.

2.1 Part (a) – Bending mode of the plate

In order to develop equations for the plate bending problems, components u and v are dropped from Eq. (1). After enforcing this condition, Eq. (1) takes the following matrix form.

$$\{u'\} = [Z_1]\{\Delta\} \tag{2}$$

where $\{u'\}^T = \{u' \ \ v' \ \ w'\}$, $\{\Delta\}^T = \{w \ \ \beta_1 \ \ \beta_2\}$ and $[Z_1] = \begin{bmatrix} 0 & z & 0 \\ 0 & 0 & z \\ 1 & 0 & 0 \end{bmatrix}$.

The strain-displacement relationship is derived as:

$$\{\varepsilon'\} = [Z]\{X\} \quad \text{and} \quad \{X\} = [d]\{\Delta\} \tag{3}$$

where

$$\{\varepsilon'\}^T = \{\varepsilon'_x \ \ \varepsilon'_y \ \ \gamma'_{xy} \ \ \gamma'_{yz} \ \ \gamma'_{zx}\}$$

$$\{X\}^T = \{\gamma_{zx} \ \ \gamma_{yz} \ \ k_x \ \ k_y \ \ k_{xy}\}$$

$$\gamma_{yz} = \frac{\partial w}{\partial y} + \beta_2, \quad \gamma_{zx} = \frac{\partial w}{\partial x} + \beta_1 \tag{4}$$

$$ak_x = \frac{\partial \beta_1}{\partial x}, \quad ak_y = \frac{\partial \beta_2}{\partial y}, \quad ak_{xy} = \frac{\partial \beta_1}{\partial y} + \frac{\partial \beta_2}{\partial x}$$

$$[Z] = \begin{bmatrix} 0 & 0 & z & 0 & 0 \\ 0 & 0 & 0 & z & 0 \\ 0 & 0 & 0 & 0 & z \\ 1 & 0 & 0 & 0 & 0 \\ 0 & 1 & 0 & 0 & 0 \end{bmatrix}; \quad [d]^T = \begin{bmatrix} \frac{\partial}{\partial x} & \frac{\partial}{\partial y} & 0 & 0 & 0 \\ 1 & 0 & \frac{\partial}{\partial x} & 0 & \frac{\partial}{\partial y} \\ 0 & 1 & 0 & \frac{\partial}{\partial y} & \frac{\partial}{\partial x} \end{bmatrix}$$

In the above equation, displacement (w) and coordinates (x, y) are normalized with respect to one of the principal dimensions of the plate, either the length (a) or the width (b) of a rectangular plate.

This provides a non-dimensional form to the above equations.

Strain energy under the given state of stress (or strain) for an infinitesimal volume $dx\,dy\,dz$ is given by

$$dU = \frac{1}{2}\{\varepsilon'\}^T[E]\{\varepsilon'\}dxdydz = \frac{1}{2}\{X\}^T[Z]^T[E]\{Z\}\{X\}dxdydz \tag{5}$$

where matrix $[E]$ is the fifth order and composed of the elastic modulus (E) and the Poisson's ratio (ν). The non-zero terms of $[E]$ are as follows.

$$E_{11} = E_{22} = \frac{E}{1-\nu^2}, \quad E_{12} = E_{21} = \nu E_{11}, \quad E_{33} = \frac{E}{2(1+\nu)}, \quad \text{and}$$
$$E_{44} = E_{55} = k_{scf}E_{33} \tag{6}$$

The shear correction factor (k_{scf} = 5/6) is used in the matrix to compensate for the parabolic distribution of the transverse shear stress along the thickness of the plate. Integration of Eq. (5) over the thickness of the plate, gives

$$U = \frac{1}{2}\iint_{Area}\{X\}^T[D]\{X\}dxdy \tag{7}$$

where $[D]_{5\times5}$ is composed of the geometric and elastic properties of the plate.

$$[D] = \int_{-\frac{h}{2}}^{+\frac{h}{2}}[Z]^T[E][Z]dz \tag{8}$$

The non-zero terms in $[D]_{5\times5}$ are given below.

$$D_{11} = D_{22} = k_{scf}\left(\frac{1-\nu}{2}\right)K_0, \quad D_{33} = D_{44} = D_0$$
$$D_{34} = D_{43} = \nu D_0, \quad D_{55} = \left(\frac{1-\nu}{2}\right)D_0$$
$$K_0 = \frac{Eh}{1-\nu^2}, \quad D_0 = \frac{Eh^3}{12(1-\nu^2)} \tag{9}$$

A numerical solution procedure is developed in this investigation for the buckling analysis of plates. The method is described below in various steps.

A quadrilateral region representing the middle plane of the plate with four straight edges defines the geometry of the plate in x-y plane as shown in Fig. 1. The thickness (h) of the plate is assumed to be uniform and small in comparison with the other dimensions along the x and y axes. The coordinates (x_i, y_i) with i = 1, 2, 3, and 4 of the four geometric nodes at the middle plane are prescribed. The shape functions $N_i(\xi, \eta)$ with i = 1, 2, 3, and 4 are used below in Eq. (10) for the interpolation of coordinates (x, y) of an arbitrary point inside the quadrilateral region in which the dimensionless natural coordinates are bounded by $-1 \leq (\xi, \eta) \leq +1$, (Weaver and Johnson 1984).

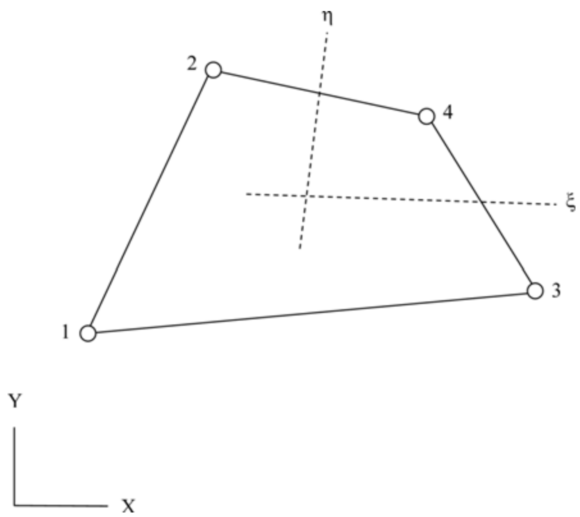

Fig. 1 A quadrilateral boundary represented by 4 points

$$x(\xi, \eta) = \sum_{i=1}^{4} N_i(\xi, \eta) x_i$$

$$y(\xi, \eta) = \sum_{i=1}^{4} N_i(\xi, \eta) y_i \tag{10}$$

The displacement field is defined by high order polynomials in comparison with the ones used for the geometric interpolation in Eq. (10). Only one displacement field defines the displacement components (w, β_1, β_2) in the whole region of the plate. In other words the high order polynomials represent the displacement field of the whole plate as one element. A different set of equally spaced nodes is created using Eq. (10) and each node has three degrees of freedom corresponding to w, β_1, and β_2. Using the (x, y) coordinates of the displacement nodes, the following is obtained.

$$w = \sum_{i=1}^{n} f_i(x, y) W_i; \quad \beta_1 = \sum_{i=1}^{n} f_i(x, y) \theta_i; \quad \beta_2 = \sum_{i=1}^{n} f_i(x, y) \phi_i \tag{11}$$

In the above equations, $f_i(x, y)$ is the displacement shape function and the indices W_i, θ_i, and ϕ_i correspond to w, β_1, and β_2 respectively at the ith displacement node. If p and q denote the orders of the polynomials in x and y respectively, the number of displacement nodes required is: $n = (p + 1)(q + 1)$. Eq. (11) can be expressed in matrix form as

$$\{\Delta\} = [\bar{F}(x, y)]\{\Gamma\} \tag{12}$$

where $\{\Delta\}^T = \{w \ \ \beta_1 \ \ \beta_2\}$,

$$\{\Gamma\}^T = \{W_1 \ \ \theta_1 \ \ \phi_1 \ \ W_2 \ \ \theta_2 \ \ \phi_2 \ \ - \ - \ - \ \ W_n \ \ \theta_n \ \ \phi_n\} \quad \text{and}$$

$$[\bar{F}(x, y)]_{3 \times 3n} = [[F_1(x, y)] \ \ [F_2(x, y)] \ \ [F_3(x, y)] \ \ - \ - \ \ [F_n(x, y)]]$$

Matrix $[F_i(x, y)]_{3 \times 3}$ in which $i = 1, 2, 3, \ldots, n$, is given below.

$$[F_i(x, y)] = \begin{bmatrix} f_i(x, y) & 0 & 0 \\ 0 & f_i(x, y) & 0 \\ 0 & 0 & f_i(x, y) \end{bmatrix} \tag{13}$$

Using Eq. (12) into Eq. (3), the following is obtained.

$$\{X\} = [d][\bar{F}(x, y)]\{\Gamma\} = [B]\{\Gamma\} \tag{14}$$

where $[B]_{3 \times 3n} = [d][\bar{F}(x, y)]$ and is not presented in its detailed form because of large size. Now, substituting Eq. (14) into Eq. (7), the strain energy expression can be written as

$$U = \frac{1}{2}\{\Gamma\}^T[K]\{\Gamma\} \tag{15}$$

Here matrix $[K]$ represents the stiffness matrix of the whole plate and is given by

$$[K] = \iint_{Area} [B]^T[D][B]dydx \tag{16}$$

To calculate the stiffness matrix $[K]$, the integration will be carried out numerically over the entire domain of the plate using the Gauss-method, in which the analyst has to decide on the number of Gauss points to be used in the process. Size of the grid consisting of the integration points, or the Gauss points, depends on the orders of polynomials that have been used in the displacement field (Eq. (11)). In Eq. (16), matrix $[D]$ is constant as it is made up of the thickness and the elastic properties of the plate. Matrix $[B]$ along with $[B]^T[D][B]$ needs to be calculated at each integration point. Then the product of the matrices is multiplied by the weight factors also associated with an integration point and added to get the final stiffness matrix $[K]$.

2.2 Part (b) – Extensional mode of the plate

In this section, the derivation of the stiffness matrix for a plate subject to in-plane loading condition is described briefly. For this case, β_1, β_2 and w are dropped from the displacement field. The in-plane displacement fields corresponding to u and v respectively in the x and y directions are taken in the same form as above for the β_1, β_2 and w.

$$u = \sum_{i=1}^{n} f_i(x, y)U_i \quad \text{and} \quad v = \sum_{i=1}^{n} f_i(x, y)V_i \tag{17}$$

Through the use of the elasticity equations, i.e., strain displacement relationship, Hooke's law, strain energy, work done by the applied forces under the assumed state of deformation etc., for the plane-stress conditions, the stiffness matrix and the load vector can be derived following the procedure similar to the above. With these, the plate can be analyzed and its state of stress under a given loading and boundary conditions can be obtained. It will be used in the buckling load calculation in the following section.

3. Buckling analysis

A method to obtain the bucking load is discussed in this section for a plate bounded by four straight edges as shown in Fig. 1 and subjected to distributed compressive loads on edges 1-2 and 3-4 in the direction of the x-axis such that the plate is in equilibrium. Under this load on an arbitrary shaped plate, it is obvious that the distribution of σ_x will be uneven over the middle surface of the plate. For the linear elastic problem, the work done by the in-plane force on the plate can be written by the following equivalent strain-energy equation (Bulson 1970).

$$T = \frac{1}{2}h \iint_{Area} \left[\sigma_x(x,y)\left(\frac{\partial w}{\partial x}\right)^2 + 2\sigma_{xy}(x,y)\left(\frac{\partial w}{\partial x}\frac{\partial w}{\partial y}\right) + \sigma_y(x,y)\left(\frac{\partial w}{\partial y}\right)^2 \right] dx\,dy$$

In matrix form the above is

$$T = \frac{1}{2}\{\Gamma\}^T \iint_{Area} [B_w]^T (h[\sigma])[B_w]dxdy\{\Gamma\} = \frac{1}{2}\{\Gamma\}^T[K_L]\{\Gamma\} \tag{18}$$

where σ_x and σ_y are the normal stresses in the x and y directions respectively, while σ_{xy} is the shear stress in the x-y plane. Vector $\{\Gamma\}$ has been defined in Eq. (12) and the load matrix is:

$$[K_L] = \iint_{Area} [B_w]^T (h[\sigma])[B_w]dxdy \tag{19}$$

The other matrices are presented below.

$$[\sigma] = \begin{bmatrix} \sigma_x & \sigma_{xy} \\ \sigma_{xy} & \sigma_y \end{bmatrix}; \quad \begin{Bmatrix} \dfrac{\partial w}{\partial x} \\ \dfrac{\partial w}{\partial y} \end{Bmatrix} = [B_w]\{\Gamma\}; \quad [B_w] = [d_w][\bar{F}(x,y)]; \text{ and}$$

$$[d_w] = \begin{bmatrix} \dfrac{\partial}{\partial x} & 0 & 0 \\ \dfrac{\partial}{\partial y} & 0 & 0 \end{bmatrix} \tag{20}$$

One can simply observe that the forms of Eqs. (18) and (19) are the same as that of the strain-energy expression and stiffness matrix given in Eqs. (15) and (16) respectively. The load matrix $[K_L]$ will also be obtained via numerical integration using the Gauss method in the same manner as for the stiffness matrix calculation. Matrices $[\sigma]$, $[B_w]$ and the triple matrix product inside the integral are needed to be calculated at each integral point. The trick is that to create matrix $[\sigma]$ under a given in-plane edge stress of σ_0, the plate has to be analyzed first in the extensional mode and stresses in the $x-y$ plane have to be evaluated at each Gauss point in terms of σ_0. For convenience, the computation of numerical results can be performed with a unit stress at the edge in question.

Fig. 2 is introduced at this stage to explain the detailed integration procedure for obtaining the stiffness and load matrices. In case of a full quadrilateral plate, the middle plane is divided into three regions from: $x_1 - x_2$, $x_2 - x_4$, and $x_4 - x_3$ respectively. For example, under the given state of deformation, contributions from each of the three regions are added to get the total stiffness $[K]$ of the plate.

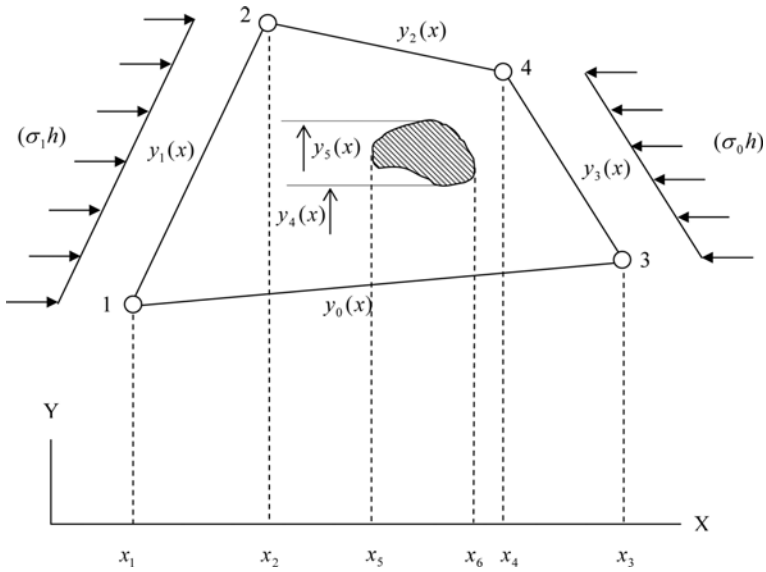

Fig. 2 Middle plane of the plate with opening showing partitioning of the area for integration

$$[K]_{FP} = \int_{x_1}^{x_2}\int_{y_0(x)}^{y_1(x)}(\ldots) + \int_{x_2}^{x_4}\int_{y_0(x)}^{y_2(x)}(\ldots) + \int_{x_4}^{x_3}\int_{y_0(x)}^{y_3(x)}(\ldots) \tag{21}$$

Similarly, the load matrix given by Eq. (19) can be obtained.

$$[K_L]_{FP} = \int_{x_1}^{x_2}\int_{y_0(x)}^{y_1(x)}(:::) + \int_{x_2}^{x_4}\int_{y_0(x)}^{y_2(x)}(:::) + \int_{x_4}^{x_3}\int_{y_0(x)}^{y_3(x)}(:::) \tag{22}$$

In the above, $(\ldots) = [B]^T[D][B]dydx$ and $(:::) = [B_w]^T(h[\sigma])[B_w]dxdy$. The subscript (FP) is used here to represent the full plate. As mentioned before, sufficiently high number of Gauss points and corresponding weights in each of the three regions has to be considered for the accurate result. For the same geometry of the plate, except that it has an opening as shown in Fig. 2 by the shaded area, the stiffness and load matrices are obtained for the opening area and are given in the following.

$$[K]_H = \int_{x_5}^{x_6}\int_{y_4(x)}^{y_5(x)}[B]^T[D][B]dydx \quad \text{and}$$

$$[K_L]_H = \int_{x_5}^{x_6}\int_{y_4(x)}^{y_5(x)}[B_w]^T(h[\sigma])[B_w]dydx \tag{23}$$

The net stiffness and load matrices for the plate with an opening are:

$$[K]_e = [K]_{FP} - [K]_H \quad \text{and} \quad [K_L]_e = [K_L]_{FP} - [K_L]_H \tag{24}$$

In the above, the subtraction of the stiffness matrix corresponding to the hole from the stiffness matrix of the full plate can be taken in the sense that the hole introduces negative stiffness to the plate system. The sum of strain energy of the plate and the work done by the load on the plate is its potential energy which as an expression is: $\Pi = U + T$. Taking the variation of the potential energy, one can easily derive the following equilibrium equation.

$$([K]_e + \sigma_{cr} h [K_L]_e)\{\Gamma\} = 0 \tag{25}$$

Eq. (25) is an eigen-value problem and at critical condition σ_0 has been replaced by σ_{cr}. The solution of this equation gives the eigen-values at different modes, which are the critical buckling loads.

4. Numerical results and discussion

A doubly connected rectangular plate having length a and width b as shown in Fig. 3 is considered for the linear buckling analysis using the method presented in this paper. The irregular shaped opening is defined by (x_0, y_0) as its geometric centre and c and d as length and width along the x and y axes respectively. The plate is assumed to be subjected to a uniform load in compression at the two opposite edges in the x direction. The plate is first analyzed in the plane stress condition under which only in-plane deformation components u and v are considered in the x and y directions respectively. The in-plane stresses are computed from this part of analysis so that they can be used in the calculation of the buckling load matrix $[K_L]$. For the buckling analysis, the stiffness matrix $[K]$ is obtained for the first order shear deformable plates with and without holes using (w, β_1, β_2) displacement parameters. Two boundary conditions, viz. all edges simply supported and all edges fully clamped respectively are considered in this paper and listed in the following.

<u>Simply Supported Edge Condition</u>: $w = \beta_2 = 0$ on the vertical edges and $w = \beta_1 = 0$ on the horizontal edges of the rectangular plate shown in Fig. 3.

<u>Fully Fixed Edge Condition</u>: $w = \beta_1 = \beta_2 = 0$ on all four edges.

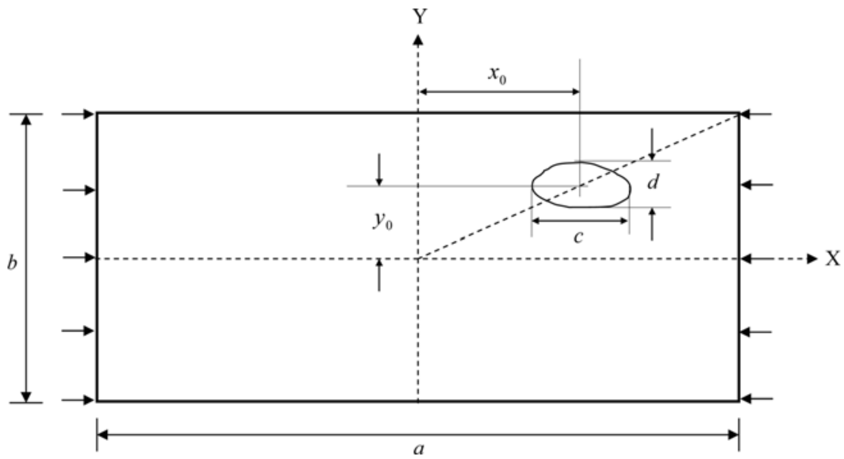

Fig. 3 A rectangular plate, with an arbitrary shaped hole at (x_0, y_0), subjected to uniform uniaxial compressive loading on two opposite edges

The above conditions are satisfied using the degrees of freedom (w, β_1, β_2) at the displacement nodal points which fall on the edges.

Object oriented C++ has been used to develop the computer program with double precision. As discussed earlier in this paper, the negative matrices: corresponding to in-plane stiffness, the bending stiffness and buckling load, are used for the plate with an opening. The geometry of the rectangular plate is defined by 4 points and the same number of shape functions. Linear polynomials in each directions are used in Eq. (10). The same equation is then used to find the Cartesian coordinates of the displacement grid points corresponding to which the displacement shape functions referred in Eq. (11) are generated using the same order of interpolating polynomials in both x and y directions. The critical buckling loads $(\sigma_{cr}h)$ per unit length along the edge and corresponding deformed shape are calculated by solving for the eigen-value and eigen-vector of Eq. (25). Then the buckling coefficient k, which is a dimensionless parameter and introduced in the following equation is found and presented in this paper.

$$k = \frac{(\sigma_{cr}h)b^2}{\pi^2 D_0} \tag{26}$$

4.1 Convergence study

Before the present method is used to analyze the plates with or without holes, a convergence study is carried out to examine the strength and the weakness of the method. A plate simply supported on all edges with a circular hole at its geometric centre, i.e., $x_0 = y_0 = 0$ and considering $c = d =$ diameter in Fig. 3 for the opening, is used for this purpose. The buckling coefficient k is calculated for four cases with $(d/b) = 0.0$, 0.10, 0.20, and 0.50 and plotted against the order of the polynomials, as shown in Fig. 4. For the full rectangular plate represented by $(d/b) = 0.0$, the convergence is rapid and at 7th order of the polynomials the result reaches the exact value of 4.00. Convergence is rapid and stable also for the plate with $(d/b) = 0.10$. Then the results start oscillating as the opening gets bigger in size and this becomes quite prominent in Fig. 4 for the case with

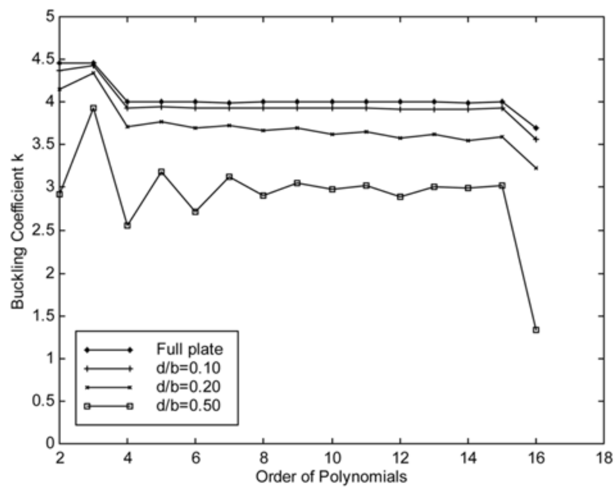

Fig. 4 Convergence study on a simply supported square plate with a circular hole at the center

$(d/b) = 0.50$. This oscillatory behavior is of relatively minor significance for the case with $(d/b) = 0.20$. The method presented in this paper involves a single displacement field for the entire domain. It is obvious that the distributions of displacement components and the resulting stresses become very complex if the hole size is big. It is anticipated by the authors of this paper that this kind of oscillation can be due to computational algorithm used for numerical integration and/or obtaining the eigen values and associated eigen vectors and not the method itself. The present method yields exact result for the full plate. In order to get stable results, the values of buckling coefficients obtained by using 9th, 10th, 11th, and 12th orders of the displacement polynomials are averaged in this paper for the cases considered in the following sections, except for the plate without a cutout.

4.2 Comparison with the exact method

Simply supported and clamped rectangular plates subjected to uniform compressive axial loading in the x direction on two opposite edges as shown in Fig. 3 are analyzed so that the present results can be compared with the exact results available in the monograph of Timoshenko and Gere (1961). The exact expression for the buckling coefficient for the simply-supported case from (Timoshenko and Gere 1961) is given by

$$k = \frac{a^2 b^2}{m^2}\left(\frac{m^2}{a^2} + \frac{n^2}{b^2}\right)^2 \tag{27}$$

Here m represents the number of half-waves in the x-direction while n is the number of half-waves in the y-direction. The displacement fields for the rectangular plates in each of the x and y directions are defined by the 10th and 12th order polynomials for simply supported and clamped edge cases respectively. The number of displacement nodes required for the 10th order polynomial is 121 and the size of the matrices solved to obtain the buckling coefficient is three times this value as each displacement grid point has three degrees of freedom (w, β_1, β_2). Similarly, for the 12th order polynomial used in the case of the clamped plate, there are 169 displacement nodes with matrix size of 507. Unlike stiffness matrix, which is full with very few zeros, the buckling load matrix contains zeros in the rows and columns pertaining to β_1 and β_2 while the size of this matrix is kept the same as that of the stiffness matrix. The displacement restraints are applied only to those nodes that lie on the boundary of the plate.

Table 1 contains the values of the buckling coefficient k obtained from the present method as well as Eq. (27) for the simply supported rectangular plate for: $m = 1 - 5$ and $n = 1 - 3$ and different values of a/b ratio from 0.25 to 3.0. It is seen in Table 1 that the buckling coefficient k increases with the value of n for a given m. The present results are in excellent agreement with the exact solution. For a given value of m, k begins with a high value at low aspect ratio and decreases to a minimum and then starts increasing. For the cases with $n = 1$, the lowest value of the buckling coefficient is 4.00 for aspect ratios $a/b = 1$, 2 and 3. Also the value of the buckling coefficient k is repeated for different aspect ratios as well as m and n. For example: when $n = 1$, $k = 18.06$ is repeated for $m = 1$, 2, and 3 for aspect ratios $a/b = 0.25$, 0.50, and 0.75 respectively. Similarly, with the same values of m and aspect ratios just mentioned, the values of k are found to be 25.0 and 39.06 for $n = 2$ and $n = 3$ respectively. This trend is repeated further and can be seen in Table 1.

Table 1 Buckling coefficient values for rectangular plates with simply supported edges. PM – Present Method

Values of buckling coefficient (***K***)							
n		1		2		3	
a/b	*m*	PM	Exact Sol.	PM	Exact Sol.	PM	Exact Sol.
0.25	1	17.98	18.06	24.86	25.00	38.79	39.06
	2	64.83	66.02	70.89	72.25	81.59	83.27
	3	146.02	146.01	155.84	152.11	162.53	162.56
	4	255.56	258.00	262.96	264.06	268.74	274.32
	5	405.50	402.00	405.50	408.04	405.50	418.20
0.50	1	6.24	6.25	15.96	16.00	42.10	42.25
	2	17.98	18.06	24.86	25.00	38.79	39.06
	3	37.64	38.03	43.95	44.44	55.55	56.25
	4	64.95	66.02	71.01	72.25	81.70	83.27
	5	101.86	102.01	105.73	108.16	115.91	118.81
0.75	1	4.34	4.34	18.75	18.78	65.14	65.34
	2	9.23	9.25	17.31	17.36	36.34	36.50
	3	17.98	18.06	24.86	25.00	38.79	39.06
	4	30.29	30.48	36.73	37.01	48.83	49.29
	5	46.18	46.47	52.39	52.80	63.61	64.27
1.0	1	4.00	4.00	24.96	25.00	99.72	100.00
	2	6.24	6.25	15.96	16.00	42.10	42.25
	3	11.08	11.11	18.71	18.78	35.82	36.00
	4	18.01	18.06	24.96	25.00	38.82	39.06
	5	27.01	27.04	33.54	33.64	45.96	46.24
1.25	1	4.20	4.20	33.60	33.64	145.20	145.20
	2	4.95	4.95	16.78	16.81	52.20	52.20
	3	7.92	7.93	16.49	16.54	37.82	37.82
	4	12.32	12.34	19.74	19.80	36.15	36.15
	5	18.09	18.06	24.97	25.00	39.06	39.06
1.5	1	4.69	4.69	44.39	44.44	200.69	200.69
	2	4.34	4.34	18.75	18.78	65.34	65.34
	3	6.24	6.25	15.96	16.00	42.25	42.25
	4	9.25	9.25	17.32	17.36	36.50	36.50
	5	13.23	13.20	20.54	20.55	36.40	36.40
1.75	1	5.39	5.39	57.26	57.33	266.39	266.39
	2	4.07	4.07	21.52	21.56	81.32	81.32
	3	5.27	5.28	16.35	16.38	48.50	48.50
	4	7.41	7.42	16.25	16.29	38.73	38.73
	5	10.32	10.29	18.11	18.12	36.09	36.09
2.0	1	6.25	6.25	72.16	72.25	342.25	342.25
	2	4.00	4.00	24.96	25.00	100.00	100.00
	3	4.69	4.69	17.33	17.36	56.25	56.25
	4	6.25	6.25	15.97	16.00	42.25	42.25
	5	8.44	8.41	16.80	16.81	37.21	37.21
3.0	1	11.11	11.11	151.93	152.11	747.11	747.11
	2	4.69	4.69	44.39	44.44	200.69	200.69
	3	4.00	4.00	24.96	25.00	100.00	100.00
	4	4.34	4.34	18.75	18.78	65.34	65.34
	5	5.15	5.14	16.50	16.54	49.94	49.94

Table 2 Bucking coefficient values for rectangular plates with built in edges. PM-Present Method

a/b	PM K	Exact Sol. K
0.75	11.63	11.69
1.00	10.05	10.07
1.25	9.24	9.25
1.50	8.33	8.33
1.75	8.09	8.11
2.00	7.85	7.88
2.25	7.61	7.63
2.50	7.56	7.57
2.75	7.43	7.44
3.00	7.35	7.37
3.25	7.34	7.35
3.50	7.26	7.27
3.75	7.24	7.24
4.00	7.26	7.23

Table 2 contains the lowest mode values of k for the clamped rectangular plates for different a/b ratios from 0.75 to 4.0. Here in this case the values of k decrease with the increase in (a/b). The results from Tables 1 and 2 show that plates with lower aspect ratios are relatively stiffer than those having higher aspect ratios. In both tables the results from the present method are in excellent agreement with the exact results (Timoshenko and Gere 1961).

4.3 Comparison with the finite element methods

In this section cases are presented so that the results from the present method and the finite element methods can be compared. In the first case, a simply supported square plate having a square hole at the center is analyzed by the authors using the present method and the FE code I – DEAS. This case was also reported by El-Sawy and Nazmy (2001) who used ANSYS for the analysis. Fig. 5 shows three plots of the buckling coefficient (k) against the hole size (d/b). The curve with solid line represents the present method. Similarly, the curves with symbols (o) and (x) represent respectively the results from the finite element codes ANSYS used by El-Sawy and Nazmy and I – DEAS used by the authors of this paper. The hole sizes from d/b = 0.0 – 0.70 were used in the calculation. The present method yields slightly higher values for k than the finite element methods and maximum difference between the present and finite element results is less than 5 percent. The authors of this paper also carried out convergence study with I-DEAS, but it is not included in the paper. Calculations using I-DEAS were performed with 256 eight node elements, each node with six degrees of freedom and the total number of nodes in the model was 866.

The second case deals with the calculation and comparison of the buckling coefficient of a simply supported square plate with a circular hole. Calculations are carried out for five different hole sizes: d/b = 0.10, 0.20, 0.30, 0.40, and 0.50 and also the location of the hole is moved along the x-axis of the plate from the centre to the right side edge. Results are plotted in Fig. 6 against (x_0/b),

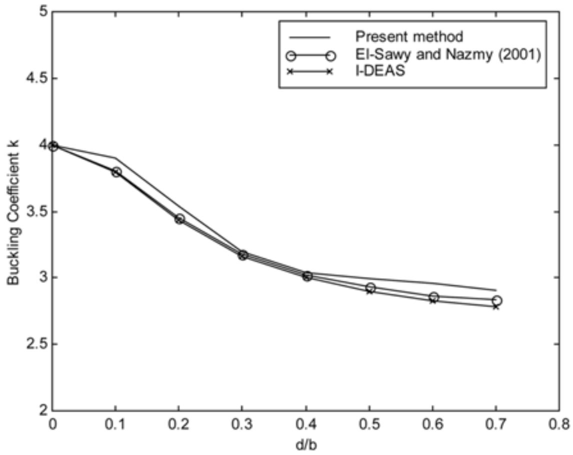

Fig. 5 Comparison between the buckling coefficient values from the present method and El-Sawy and Nazmy (2001) and I-DEAS for a simply supported square plate with a square hole at the center

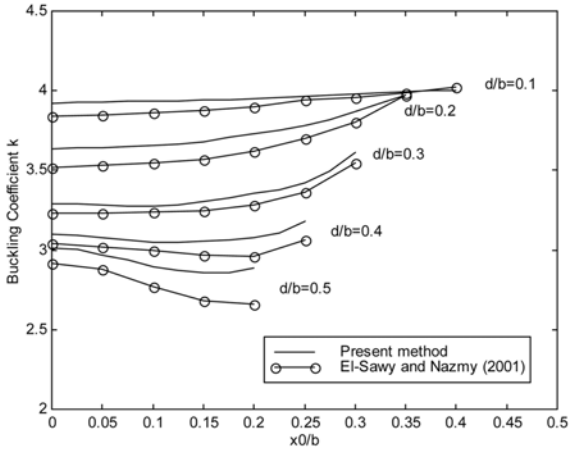

Fig. 6 Comparison between buckling coefficient values from present method and El-Sawy and Nazmy (2001) for a simply supported square plate with a circular hole moving along the x-axis from the center

representing the hole positions from the center, for the above five hole sizes. In this figure, results from the present method are shown by the solid lines and those from the work of El-Sawy and Nazmy (2001) by the solid lines with symbol (o). The trend in the variation of the buckling coefficient for both cases is very similar. Difference between the results from the two sources increases with the hole size and the maximum being in the neighborhood of eight percent for the largest hole with d/b = 0.5.

The present method is further applied to simply supported square plate with a circular hole at the centre and the results are presented in Table 3 which also contains results from the I-DEAS and the percentage difference between the results. Comparison here is very good and the maximum difference is less than seven percent for the hole size d/b = 0.70. The error is significantly higher in the vicinity of thirteen percent for the case with d/b = 0.80. This size of hole in a plate is definitely

Table 3 Values of buckling coefficient k for square plate with a circular hole located at the center of the plate. PM – Present Method

d/b	Buckling coefficient (k)		
	PM	I-DEAS	%-Difference
0.0	4.00	4.00	0.00
0.1	3.92	3.84	2.08
0.2	3.64	3.51	3.70
0.3	3.29	3.22	2.17
0.4	3.10	3.03	2.31
0.5	3.01	2.90	3.79
0.6	2.95	2.81	4.98
0.7	2.90	2.72	6.62
0.8	2.95	2.62	12.60

Table 4 Values of buckling coefficient k for square plate with an elliptic hole eccentrically located in the plate. PM – Present Method

x_0/b, y_0/b	Buckling coefficient k			
	Square plate with elliptic hole c/b = 0.150, d/b = 0.10			
	Simply supported		Fully clamped	
	PM	I-DEAS	PM	I-DEAS
0.25, 0.25	3.94	3.88	9.95	9.91
0.25, 0.00	3.94	3.86	10.19	10.24

impractical with regards to its application. Square plates with an elliptical hole of c/d = 1.5 and d/b = 0.10 is also analyzed for simply supported and clamped boundary conditions. Two hole locations with (x_0/b, y_0/b) values of (0.25, 0.25) and (0.25, 0.0) respectively are considered and the results are compared with the same from I-DEAS as shown in Table 4 with maximum difference of two percent.

4.4 Rectangular plate with circular opening

In the above cases, numerical results for the square plate with an opening were calculated by the present and the FE methods. In this section, some additional results from the present method are presented for rectangular plates with a circular opening, the location of which is varied along the diagonal. Both simply supported and fixed boundary conditions were investigated. Figs. 7-10 show results for the simply supported rectangular plate for four aspect ratios of a/b = 1.0, 2.0, 3.0 and 4.0 and each figure has six graphs corresponding to d/b = 0.05, 0.10, 0.15, 0.20, 0.25 and 0.30. Similarly, Figs. 11-14 contain results for the clamped boundary condition with the above aspect ratios and hole diameters. The values of the buckling coefficient (k) are plotted against (x_0/b) which represents the normalized x-coordinate of the center of the hole. Generally, the value of the bucking

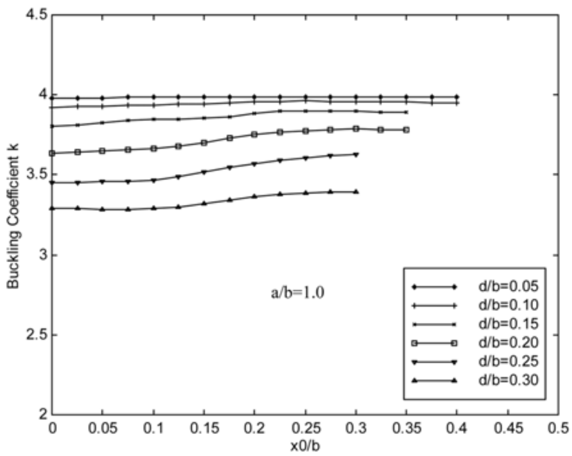

Fig. 7 Buckling Coefficient (k) for a simply supported plate of a = b with a circular hole moving along the diagonal of the plate from the center to the loaded edge

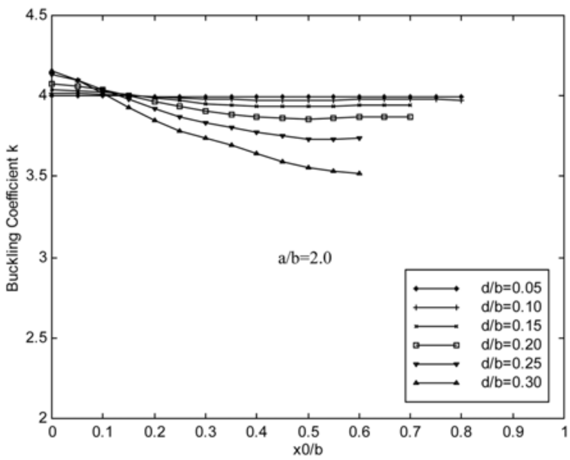

Fig. 8 Buckling Coefficient (k) for a simply supported plate of a = $2b$ with a circular hole moving along the diagonal of the plate from the center to the loaded edge

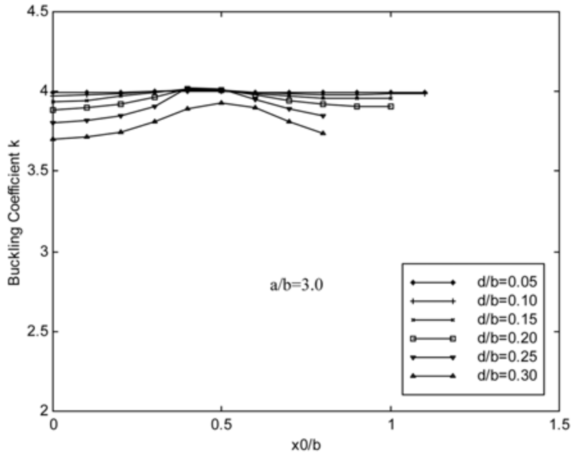

Fig. 9 Buckling Coefficient (k) for a simply supported plate of a = 3b with a circular hole moving along the diagonal of the plate from the center to the loaded edge

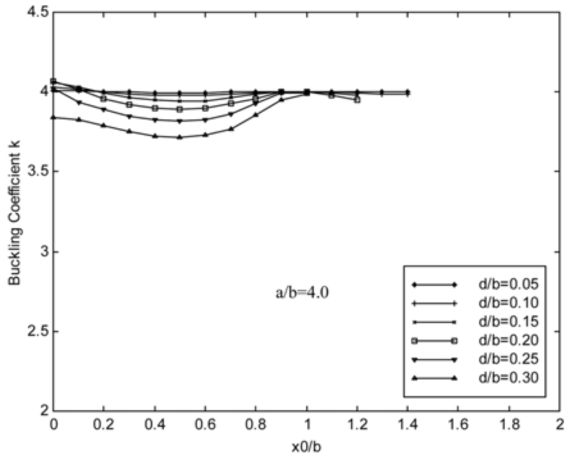

Fig. 10 Buckling Coefficient (k) for a simply supported plate of a = 4b with a circular hole moving along the diagonal of the plate from the center to the loaded edge

coefficient decreases with the increase in the hole diameter. One can easily notice in Table 1 that the lowest buckling mode for each of the aspect ratios 1.0, 2.0 and 3.0 occurs at k = 4.0. Also noticed in Figs. 7-10 is that the buckling coefficients for small hole with d/b = 0.05 and 0.10 are very close to 4.00 for all aspect ratios of 1 through 4. This is consistent with the fact that small holes do not considerably alter the buckling behavior of the plate. The plate behaves more or less like a solid plate without an opening. For square plate, the buckling coefficients decrease with the increasing hole diameter regardless of the location of the hole with respect to the geometric center.

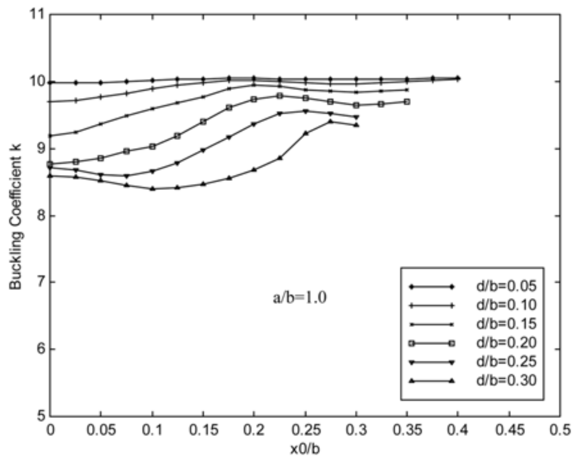

Fig. 11 Buckling Coefficient (k) for a built in plate of a = b with a circular hole moving along the diagonal of the plate from the center to the loaded edge

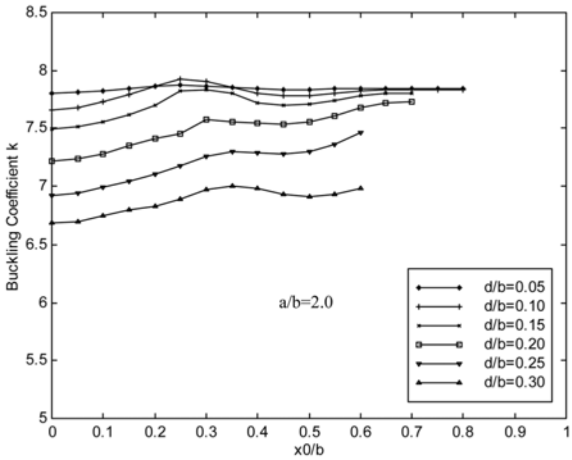

Fig. 12 Buckling Coefficient (k) for a built in plate of a = 2b with a circular hole moving along the diagonal of the plate from the center to the loaded edge

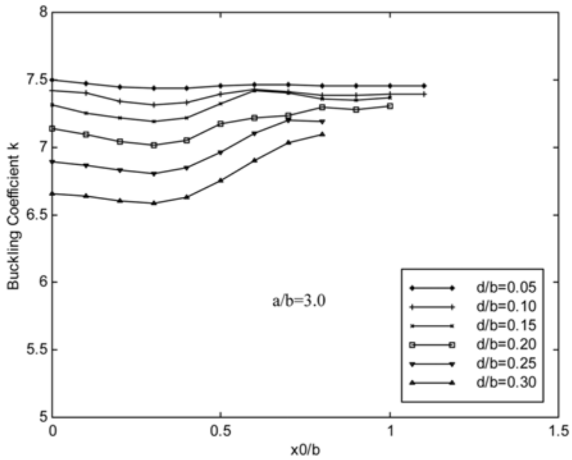

Fig. 13 Buckling Coefficient (k) for a built in plate of a = 3b with a circular hole moving along the diagonal of the plate from the center to the loaded edge

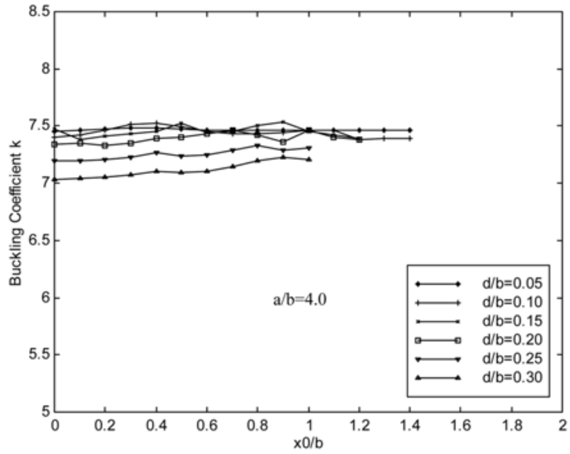

Fig. 14 Buckling Coefficient (k) for a built in plate of a = 4b with a circular hole moving along the diagonal of the plate from the center to the loaded edge

It is consistent with the logic that large size hole in a plate for a given boundary condition decreases the overall buckling strength of the plate. This decrease in the value of the buckling coefficient with increasing hole diameter is also quite significant for the cases corresponding to Figs. 8-10, if $d/b \geq 0.2$. Case with a/b = 2.0 shows behavior that is different from that of the square plate. In this case, the values of k for the plate with a hole at the center are greater than 4.0. Similar behavior is observed for the case with a/b = 4.0 in Fig. 10. The buckling strength for the cases with a/b = 3.0 and 4.0 shows a peaking tendency in the vicinities of x_0/b = 0.5 in Fig. 9 and x_0/b = 1.0 in Fig. 10 respectively. The variation of the buckling coefficient (k) for built in edge conditions of the rectangular plate against the hole position is similar in the sense that the buckling strength generally decreases with the increasing hole diameter. For small hole, the buckling coefficients are nearly constant against x_0/b with values close to 10.07, 7.88, 7.37 and 7.23 respectively for the four aspect ratios as shown in Figs. 11-14. It is also seen in Table 2 in which the comparison of the present results are made with those of the exact solution. As the aspect ratio increases, the value of k decreases. For the case shown in Fig. 14, the variation of k against x_0/b is erratic for small diameter holes having $d/b \leq 0.2$.

5. Conclusions

A single domain variational method is presented for the analysis of doubly connected plates. In this method the displacement field for the entire plate model is defined by high order polynomials while linear polynomials are used to define the boundary of the plate. In this numerical method, the integration is carried out using as many Gauss points as needed according to the order of the polynomial used for the displacement field. The method is subjected to various tests like: convergence study, comparison of the results with the exact solution, and comparison with the results from the finite element methods. Numerical examples are presented for the cases of all sides simply supported and also all sides fixed rectangular plates with or without holes. Excellent comparisons of the numerical results are made with the exact solution found in the monograph of Timoshenko and Gere (1961) and also with the finite element methods. A parametric study is also done for the rectangular plates with an opening by moving the opening from the centre of the plate along the diagonal. Different aspect ratios (a/b) and the hole sizes are considered in this study. The aspect ratio and hole size and its location greatly affect the stability of the square plate. The buckling coefficient k hardly changes with respect to position of the hole along the diagonal and the aspect ratio of the simply supported plates for very small holes, e.g. (d/b) < 0.10. If the hole is very large, i.e., the diameter being in the neighborhood of 80 percent of the length of the square plate, the difference between the results from the present method and the FEM is found to be 12.5 percent. For other cases, this difference is less than 8 percent. In the opinion of the authors, results from both methods mentioned above is questionable with regards to the accuracy for the near extreme case with 80 percent hole diameter.

References

Belytschko, T., Lu, Y.Y. and Gu, L. (1994), "Element free Galerkin methods", *Int. J. Numer. Meth. Eng.*, **37**, 229-256.

Belytschko, T., Krongauz, Y., Organ, D., Fleming, M. and Krysl, P. (1996), "Meshless method: An overview and recent developments", *Comput. Methods Appl. Mech. Eng.*, **139**, 3-47.

Bert, C.W. and Malik, D. (1996), "Free vibration analysis of thin cylindrical shells by differential quadrature method", *J. Pres. Ves. Techn.*, ASME, **118**, 1-12.

Bulson, P.S. (1970), *The Stability of Flat Plates*, Chatto and Windus, London, GB.

Chen, X.L., Liu, G.R. and Lim, S.P. (2003), "An element free Galerkin method for the free vibration analysis of composite laminates of complicated shape", *Comput. Struct.*, **59**, 279-289.

Redekop, D. and Makhoul, E. (2000), "Use of the differential quadrature method for the buckling analysis of cylindrical shell panels", *Struct. Eng. Mech.*, **10**(5), 451-462.

El Ouatouati, A. and Johnson, D.A. (1999), "A new approach for numerical modal analysis using the element-free method", *Int. J. Numer. Meth. Eng.*, **46**, 1-27.

I-DEAS Master Series™, Structural Dynamics Research Corporation, Milford, OH 45150.

El-Sawy, K.M. and Nazmy, A.S. (2001), "Effect of aspect ratio on the elastic buckling of uniaxially loaded plates with eccentric holes", *Thin-Walled Structures*, **39**, 983-998.

Mohr, G.A. (2000), "Polynomial solution for thin plates", *Int. J. Mech. Sci.*, **42**, 1197-1204.

Muhammad, T. and Singh, A.V. (2003), "A *p*-type solution for the bending of doubly connected rectangular, circular and elliptic plates", submitted to the *Int. J. Solids Struct.*

Sabir, A.B. and Chow, F.Y. (1983), "Elastic buckling of flat panels containing circular and square holes, instability and plastic collapse of steel structures", *Proc. of the Michael R. Horne Conf.*, 311-321.

Sabir, A.B. and Chow, F.Y. (1986), "Elastic buckling of plates containing eccentrically located circular holes", *Thin-Walled Structures*, **4**, 135-149.

Shakerley, T.M. and Brown, C.J. (1996), "Elastic buckling of plates with eccentrically positioned rectangular perforations", *Int. J. Mech. Sci.*, **38**, 825-838.

Suetake, Y. (2002), "Element free method based on Lagrange Polynomial", *J. Eng. Mech.*, ASCE, **128**, 231-239.

Timoshenko, S.P. and Gere, J.M. (1961), *Theory of Elastic Stability*, McGraw-Hill Book Co., INC., N.Y.

Weaver, W. and Johnston, P.R. (1984), *Finite Elements for Structural Analysis*, Prentice Hall, Englewood Cliffs, NJ.

Yettram, A.L. and Brown, C.J. (1985), "The elastic stability of square perforated plates", *Comput. Struct.*, **21**(6), 1267-1272.

Yettram, A.L. and Brown, C.J. (1986), "The elastic stability of square perforated plates under bi-axial loading", *Comput. Struct.*, **22**(4), 589-594.